Analysis of an industrial adsorption process based on ammonia chemisorption: Modeling and simulation

Cristian Cardenas, Abderrazak Latifi, Cécile Vallières, Stéphanie Marsteau, Léa Sigot

▶ **To cite this version:**

Cristian Cardenas, Abderrazak Latifi, Cécile Vallières, Stéphanie Marsteau, Léa Sigot. Analysis of an industrial adsorption process based on ammonia chemisorption: Modeling and simulation. Computers & Chemical Engineering, 2021, 154, pp.107474. 10.1016/j.compchemeng.2021.107474 . hal-03467327

HAL Id: hal-03467327
https://hal.science/hal-03467327

Submitted on 22 Aug 2023

HAL is a multi-disciplinary open access archive for the deposit and dissemination of scientific research documents, whether they are published or not. The documents may come from teaching and research institutions in France or abroad, or from public or private research centers.

L'archive ouverte pluridisciplinaire **HAL**, est destinée au dépôt et à la diffusion de documents scientifiques de niveau recherche, publiés ou non, émanant des établissements d'enseignement et de recherche français ou étrangers, des laboratoires publics ou privés.

Distributed under a Creative Commons Attribution - NonCommercial 4.0 International License

Version of Record: https://www.sciencedirect.com/science/article/pii/S0098135421002520
Manuscript_84d3e31ce373131b4d03958ed67599f7

Analysis of an industrial adsorption process based on ammonia chemisorption: modeling and simulation

Cristian Cardenas[a,b], Abderrazak M. Latifi[a,*], Cécile Vallières[a], Stéphanie Marsteau[b], Léa Sigot[a]

[a]*Laboratoire Réactions et Génie des Procédés, CNRS-ENSIC, Université de Lorraine, 1 rue Grandville, BP20451, 54001, Nancy Cedex, France*
[b]*Institut National de Recherche et de Sécurité, 1 Rue du Morvan, CS 60027, 54519, Vandoeuvre-Lès-Nancy Cedex, France*

[*]Corresponding author: abderrazak.latifi@univ-lorraine.fr

Abstract

The paper deals with the development of a one-dimensional model to simulate an industrial adsorption process of ammonia on zinc sulphate-doped activated carbon. It is described by mass balance, thermodynamic and adsorption kinetics equations. Since equilibrium is involved in the model, we started with experimental measurements of ammonia adsorption isotherms on doped activated carbon. A method based on the sensitivity analysis of parameters was used to evaluate the estimability of unknown parameters involved in the Sips adsorption isotherm equation. The estimable parameters were then identified using experimental data at three different temperatures, i.e. 285, 293 and 313 K. Experimental breakthrough fronts at different ammonia concentrations and gas flow rates were then used to determine the overall mass transfer coefficient and the axial dispersion coefficient involved in the model equations, implemented and solved within Comsol Multiphysics software. Finally, we validated the model by means of four additional breakthrough fronts that were different from those used to identify the parameters. The model predictions and the experimental measurements show a very agreement which is quantified by the performance indices of the model and confirmed by a chi-squared test. The validated model can be used as a predictive tool for the design and optimization of the ammonia adsorption process for air purification boxes used to equip cabins with pressurization and air-conditioning of mechanical devices.

Keywords: Air purification boxes, Ammonia adsorption, Doped activated carbon, Experimental measurements, Estimability analysis, Modeling and simulation

1. Introduction

The emission of gaseous ammonia is one of the main concerns of composting and organic waste methanisation facilities. Ammonia causes chronic respiratory diseases, such as asthma and occupational chronic bronchitis, when the professional exposure is too high. The Ministry of Labor (Courtois & Cadou, 2016) has established an occupational exposure limit to ammonia at 10 ppm in France.

Mechanical machinery used in composting and methanisation plants often operate in an atmosphere where the ambient level of ammonia is higher than this maximum limit. The use of mechanical devices equipped with cabin pressurization and air-conditioning is common in many fields such as building and civil engineering, waste treatment and recycling, and agriculture.

© 2021 published by Elsevier. This manuscript is made available under the CC BY NC user license
https://creativecommons.org/licenses/by-nc/4.0/

The aim of these cabins is to provide, other than working comfort, protection against various risks potentially present in the changing environment of the device, such as particles and/or gases and toxic fumes. To do so, the cabin is placed in overpressure (> 100 Pa) with respect to the outside via a filtered and purified ventilation system (Bémer et al., 2015). The air flow rate introduced into the cockpit is around 50 to 100 $m^3.h^{-1}$ depending on the manufacturer.

Currently, the installation of an air purification box is very rarely available when purchasing the machine, it is rather included as an adaptation. These air purification boxes, when they are included as protection against multiphase pollutants, are composed of a prefilter layer, followed by a high efficiency filtration layer, then an adsorbent layer. Suppliers offer various configurations, from multilayer annular cartridges to a simple overlay of adapted plane mediums. While some studies (Bémer et al., 2005; Organiscak and Schmitz, 2012) have assessed the efficiency of cabin pressurization and air-conditioning regarding protection against particles, there are little scientific or technical data on gas and vapor filter boxes. The sector with the most amount of information concerning the adsorption of dangerous gas compounds with regards to preventing occupational hazards is the respiratory personal protective equipment sector and its associated standards (Guimon, 2019).

Activated carbon is the main adsorbent material used on an industrial scale. It is mostly chosen for its large specific surface area and its low cost. Zinc sulphate-doped activated carbon is the main medium used today to equip air purification boxes for machines to purify ammonia, and where the adsorption reactions of pollutant gaseous phases take place. Currently, manufacturers assess only the performance of the adsorption layer which is generally carried out at relatively high concentration levels. The issue with evaluating the performance of purification boxes used to equip machines is complicated insomuch as the service time is very long (several days) on the one hand, and there are no or very little obligations in terms of normative testing for the purification of the gaseous phase, on the other.

The objective of this paper is to assess and improve the performance of gas and vapor purification in a pilot adsorption column containing the same zinc sulphate-doped activated carbon and operating in the same conditions as the reference air purification box. More specifically, an experimental study on adsorption of ammonia on the zinc sulphate-doped activated carbon is carried out along with the modeling of the phenomena involved in the column. The experiments mainly consist of the characterization of the doped carbon and the measurements of adsorption isotherms and breakthrough fronts of ammonia.

2. Experimental measurements

2.1. Characterisation of zinc sulphate-doped activated carbon

The doped carbon used comes from air purification boxes commercialized by the company, SP Défense. The carbon is presented in the form of grains with a diameter of around 1.5 mm. Its porous structure is experimentally defined using an isotherm carried out by adsorption manometry with liquid nitrogen at 77 K (Rouquerol et al., 2013), which enables access to essential information such as the specific surface area and the porous volume. The density of the solid or skeleton is determined by helium pycnometry. These data are summarized in *Table 1*. The average size of crystal, measured by Scanning Electron Microscopy (SEM), was 0.5 µm. All the gases (NH_3, N_2 and He) used in the experiments were provided by Air Liquide France with a purity greater than 99.999 %.

2.2. Measurements of equilibrium adsorption isotherms

For the development of the column model, adsorption isotherms of ammonia on doped activated carbon within a temperature range of 285-313 K with ammonia concentrations of up to 0.066 mol.m^{-3} were measured using a thermogravimetric analyzer from Setaram Instrumentation (SETSYS TAG). The technique involves monitoring the mass variation of a sample kept at a specific temperature when it is subjected to different concentrations of ammonia. The measurement of the mass increase has a sub-microgram resolution. The mass increase values obtained when equilibrium is achieved are converted in ammonia adsorption capacity per kg of adsorbent. Before the first measurement, primary vacuum degassing of the adsorbent was carried out at 200 °C for 15 hours.

2.3. Measurements of breakthrough fronts

The experimental adsorption rig used to measure the breakthrough fronts of ammonia is presented in *Figure 1*. Its main element is a column filled with zinc sulphate-doped activated carbon particles. The characteristics of the column as well as the operating conditions are given in *Table 2*. The gas studied is obtained by mixing compressed dry air and pure ammonia using two mass flow regulators (Brooks® Delta mass flow II) calibrated with a precision of 1 % and 0.1 % of full scale, respectively. A small column is used to ensure a mixture of ammonia and air before entering the adsorption column. Two metallic grids with fine mesh were placed at the inlet and outlet of the column to ensure an even distribution of gases and to keep the adsorbent particles in the bed.

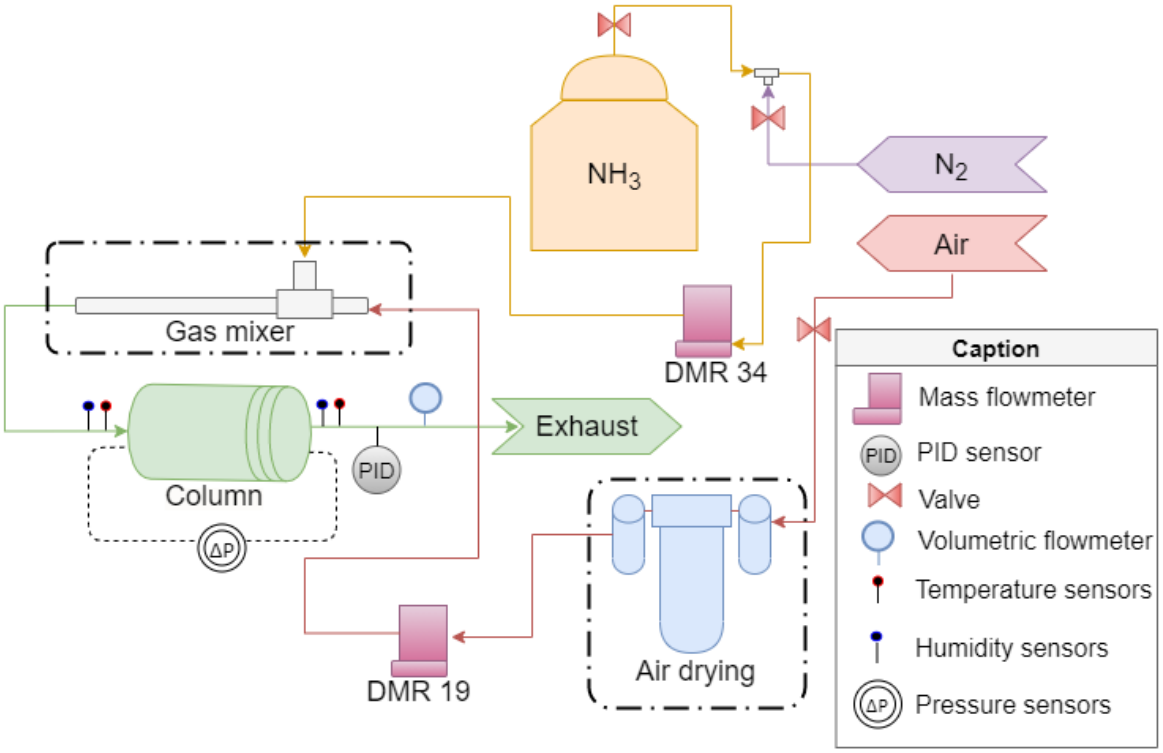

Figure 1: Experimental rig used for the measurements of breakthrough fronts

Doped activated carbon particles were used without any preliminary treatment. Temperature, pressure, and humidity sensors were placed upstream and downstream of the adsorption column. A photoionization detector (ppbRAE Plus) calibrated with a precision of 0.1 % was

used to measure the ammonia concentrations when exiting the column. All the sensors were connected to an acquisition module developed by the INRS IT department.

Table 1: Measured characteristics of the doped activated carbon

Zinc sulphate-doped activated carbon	**Value**
Mean radius of particles, mm	0.59
Solid density, $kg.m^{-3}$	2053
Particle porosity, $m_g^3.m_{pe}^{-3}$	0.40
Mean crystal diameter, µm	0.5
BET Specific surface area, $m^2.g^{-1}$	948
Mean macropore diameter, nm	1494
Total pore volume, $cm^3.g^{-1}$	0.33
Micropore volume, $cm^3.g^{-1}$	0.30

Table 2: Characteristics of the adsorption column and operating conditions

Packed bed column with doped activated carbon	**Value**
Column diameter, mm	32.2
Column height, mm	40.0
Bed porosity, $m_g^3.m_{col}^{-3}$	0.52
Adsorbent mass, g	22
Bed density, $kg.m^{-3}$	623
Temperature, °C	21
Total pressure, kPa	101,3

2.4. Experimental procedure

The adsorption column was filled with 22 g of doped activated carbon particles. The air from the air network was dried in a silica gel column before entering the adsorption column. The latter was kept under dry air until the column temperature (21°C) and relative humidity (5%) were stabilized. A gaseous mixture of ammonia and air was thus produced and supplied the adsorption column. Each experiment was repeated several times to check the repeatability and reproducibility of the results.

3. Model development

In the model development of the ammonia adsorption process on doped activated carbon, one of the main issues is to select the adsorption equilibrium isotherm that best describes the process. This isotherm must predict the maximum adsorbed quantity of gaseous ammonia (adsorbate) on the solid (adsorbent) depending on the temperature and the ammonia concentration. In addition, the temperature can have a negative effect on the adsorbent capacity. In order to thoroughly describe the adsorption phenomenon of ammonia on doped activated carbon, the renowned Sips adsorption model was used. It is detailed in the next section.

3.1. Sips adsorption isotherm

This semi-empirical equation describing the quantity adsorbed at equilibrium, q_e ($mol.kg^{-1}$), depending on the concentration in the gaseous phase at equilibrium, c ($mol.m^{-3}$), considers the interactions between the adsorbate molecules and the adsorbent surface with a heterogeneity factor, and is expressed as follows (Do, 1998):

$$q_e = \frac{q_m (b_s c)^{\frac{1}{s}}}{1 + (b_s c)^{\frac{1}{s}}} \quad (1)$$

with q_m, the maximum adsorbed quantity (mol.kg^{-1}):

$$q_m = q_{m0} \exp\left[\chi\left(1 - \frac{T}{T_0}\right)\right] \quad (2)$$

b_s, the equilibrium constant (m^3.mol^{-1}):

$$b_s = b_{s_0} \exp\left[\frac{Q}{R_g T_0}\left(\frac{T_0}{T} - 1\right)\right] \quad (3)$$

and s, the Sips heterogeneity factor:

$$\frac{1}{s} = \frac{1}{s_0} + \alpha\left(1 - \frac{T_0}{T}\right) \quad (4)$$

α and χ are constants. q_{m0} (mol.kg^{-1}), b_{s0} (m^3.mol^{-1}) and s_0 are the maximum quantity adsorbed, the equilibrium constant and the Sips heterogeneity factor at the reference temperature T_0 (K), respectively. Q (J.mol^{-1}) is the heat of adsorption and R_g (J.mol^{-1}.K^{-1}) is the ideal gas constant.

On the other hand, the Sips model is able to describe the ammonia adsorption phenomenon with precision, in particular for adsorbents with an adsorption energy distribution, due to their pores of varying sizes. This adsorption energy or isosteric heat of sorption can be expressed using the Van't Hoff equation as (Do, 1998):

$$(-\Delta H) = Q - (\alpha R_g T_0) s \ln(b_s c) \quad (5)$$

where ΔH (J.mol^{-1}) is the isosteric heat of sorption.

It depends on the temperature through the parameters q_m, b_s and s, and on the concentration in the gas phase. The negativity of enthalpy variations indicates that the adsorption is an exothermic process. Furthermore, the value of the isosteric heat of sorption will provide insightful information about the type of adsorption that ammonia undergoes on the doped activated carbon. In fact, a high (low) value means that ammonia is chemically (physically) adsorbed. The limit value between these two types of adsorption lies between 20 and 40 kJ/mol (Králik, 2014).

The isotherm equation (Eq.1) therefore involves six unknown parameters, i.e. q_{m0}, b_{s0}, s_0, Q, α and χ, which should be deduced from the experimental measurements.

3.2. Breakthrough fronts

A mathematical model was developed to describe the behavior of the breakthrough fronts of the dynamic adsorption of ammonia on doped activated carbon. It consists of mass balance equations, and thermodynamic, hydrodynamic, and kinetic equations. Moreover, the model was based on the following main assumptions: (i) the gas mixture obeys the ideal gas law, (ii) the pressure drop in the column is neglected, (iii) ammonia is the only adsorbed molecule, (iv) the resistance to the mass transfer through the boundary layer surrounding the solid particles is

neglected, (v) the kinetics of the mass transfer within a particle is described by means of the linear driving force (LDF) model, (vi) the equilibrium isotherm of the gas phase with the adsorbent is described by the Sips isotherm equation, (vii) the adsorbent particles are assumed to be spherical and homogeneous in size and density, (viii) the temperature of the column as well as the physical properties of the adsorbent are assumed to be constant, (ix) the column is a continuum of two phases, one solid and one gas, (x) only the axial dimension of the column is taken into account (mono-dimensional model).

In the gas phase, the ammonia mass balance is described by the following transient PDE involving diffusion, convection, and adsorption:

$$\frac{\partial c}{\partial t} - D_{ax}\frac{\partial^2 c}{\partial z^2} + \frac{\partial (vc)}{\partial z} = -\frac{1-\varepsilon_b}{\varepsilon_b}\frac{\partial \bar{q}}{\partial t} \tag{6}$$

where c (mol.m^{-3}) is the concentration of ammonia in the gas phase, $\bar{q}$ (mol.m^{-3}) is the average concentration of ammonia adsorbed in the solid phase, v (m.s^{-1}) is the interstitial gas velocity, D_{ax} (m².s^{-1}) is the axial dispersion coefficient and ε_b (m_g^3.m_{col}^{-3}) is the bed porosity.

The associated initial and boundary conditions are given as:

$* t = 0$ $\quad c = 0, \bar{q} = 0$ (7)

$* z = 0$ $\quad \frac{\partial c}{\partial z} = \frac{v}{D_{ax}}\left(c - c_{in}\right)$ (8)

$* z = L$ $\quad \frac{\partial c}{\partial z} = 0, \frac{\partial \bar{q}}{\partial z} = 0$ (9)

where c_{in} (mol.m^{-3}) is the concentration of ammonia at the column inlet.

In the solid phase which is constituted by the doped carbon particles, the kinetics of the mass transfer is approximated by means of the LDF model proposed by Glueckauf and Coates (1954) as:

$$\frac{\partial \bar{q}}{\partial t} = k_{LDF}\left(q_e^* - \bar{q}\right) \tag{10}$$

where $q_e^* = q_e \rho_s$ (mol.m^{-3}) is the concentration of ammonia in the solid phase at equilibrium, ρ_s (kg.m^{-3}) is the density of the solid constituting the activated carbon and k_{LDF} (s^{-1}) is the overall mass transfer coefficient which accounts for the contributions of gas/solid mass transfer and macropore and micropore diffusion. Taking into account the assumption (iv), k_{LDF} is expressed by means of the following equation (Ruthven, 1985):

$$\frac{1}{k_{LDF}k_H} = \frac{r_p^{\,2}}{15D_e} + \frac{r_\mu^{\,2}}{15D_\mu k_H} \tag{11}$$

where r_{pe} (m) is the mean radius of the particle, D_e (m².s^{-1}) is the effective diffusion coefficient of the adsorbate in the gas phase of the particle, k_H is Henry's equilibrium constant (low concentration), D_μ (m².s^{-1}) is the intra-crystalline diffusion coefficient, and r_μ (m) is the mean crystal radius.

It should be noted that the LDF model, which is an approximation of the second law of Fick, averages the radial concentration of the adsorbate within the particle. However, despite this approximation, the use of the LDF model often provides satisfactory results for simulations of adsorption processes, which may be explained by the fact that adsorption kinetics often have secondary impact with respect to adsorption equilibrium isotherms.

The resulting model (Eqs. (6-10)) will be analyzed, identified, and validated using the experimental measurements. It is noteworthy that since the axial dispersion increases with the flow rate, the parameters c_{m_1} and c_{m_2} (see *Table 3*) involved in the correlation of Rastegar and Gu (2017) were estimated in order to keep the same tendency. The unknown parameters of the model to be estimated from the measurements are therefore k_{LDF}, c_{m_1} and c_{m_2}.

The model equations are implemented and solved within Comsol Multiphysics ® software.

Table 3: Correlations used to estimate the model parameters

Binary or molecular diffusion, D_{AB}, ($m^2.s^{-1}$) (Brokaw, 1969) (Neufeld et al., 1972)	$D_{AB} = 2.6628\times10^{-22}\dfrac{\sqrt{T^3\dfrac{M_A+M_B}{2\times10^3 M_A M_B}}}{p_t\sigma_A\sigma_B\Omega_D}$ with: $\Omega_D = b_1\left(\dfrac{T}{\varepsilon_k}\right)^{b_2} + b_3\exp^{\left(-b_4\frac{T}{\varepsilon_k}\right)} + b_5\exp^{\left(-b_6\frac{T}{\varepsilon_k}\right)} + b_7\exp^{\left(-b_8\frac{T}{\varepsilon_k}\right)}$ where: $b_1 = 1.06036;\ b_2 = 0.15610;\ b_3 = 0.19300;\ b_4 = 0.47635;$ $b_5 = 1.03587;\ b_6 = 1.52996;\ b_7 = 1.76474;\ b_8 = 3.89411;\ \varepsilon_k = \sqrt{\varepsilon_A\varepsilon_B / k_b^2};$ $\varepsilon_A / k_b = 182.9;\ \varepsilon_B / k_b = 97;\ \sigma_A = 3.376\times10^{-10};\ \sigma_B = 3.617\times10^{-10}$
Dynamic viscosity, μ_B (Pa.s) (Brokaw, 1969) (Neufeld et al., 1972)	$\mu_B = 2.669\times10^{-6}\dfrac{\sqrt{T(M_B)10^3}}{\sigma_B^2\Omega_D}$ with: $\Omega_D = b_1\left(\dfrac{T}{\varepsilon_B / k_b}\right)^{b_2} + b_3\exp^{\left(-b_4\frac{T}{\varepsilon_B/k_b}\right)} + b_5\exp^{\left(-b_6\frac{T}{\varepsilon_B/k_b}\right)} + b_7\exp^{\left(-b_8\frac{T}{\varepsilon_B/k_b}\right)}$
Knudsen diffusion, D_K ($m^2.s^{-1}$) (Do, 1998)	$D_K = \dfrac{4}{3}r_{mp}\sqrt{\dfrac{2R_gT}{\pi M_A}}$
Effective diffusion, D_e ($m^2.s^{-1}$) (Ruthven, 1985) (Millington & Quirk, 1959)	$D_e = \varepsilon_{pe}\dfrac{D_M}{\tau_{pe}}$ with: $D_M = \left(\dfrac{1}{D_{AB}} + \dfrac{1}{D_K}\right)^{-1}$ where: $\tau_{pe} = \varepsilon_{pe}^{-1/3}$
Axial dispersion coefficient, D_{ax} ($m^2.s^{-1}$), (Rastegar and Gu, 2017)	$D_{ax} = \dfrac{v d_{pe}}{Pe'}$ with: $\dfrac{1}{Pe'} = \dfrac{0.7D_{AB}}{d_{pe}v} + \dfrac{\varepsilon_b}{c_{m_1} + c_{m_2}(Re_p)^{0.59}}$ where: $c_{m_1} = 0.18$ and $c_{m_2} = 0.008$
Gas density, ρ_g ($kg.m^{-3}$)	$\rho_g = \dfrac{p_t M_B}{R_g T}$
LDF effective mass transfer coefficient, k_{LDF} (s^{-1}) (Ruthven, 1985)	$k_{LDF} = \left(\dfrac{r_p^2 k_H}{15D_e} + \dfrac{r_\mu^2}{15D_\mu}\right)^{-1}$ with: $D_\mu = 1\times10^{-17}\ m^2.s^{-1}$ and $k_H = 2\times10^{-5}$

4. Estimability analysis and identification of parameters

In both adsorption isotherm and breakthrough front models, the unknown parameters involved should be estimated using experimental measurements. However, the question is to know whether the available measurements contain enough information to estimate all the unknown parameters or only part of them. To answer this question, we carried out a parameter estimability analysis based on the sensitivities of the measured outputs with respect to the parameters. The objective is to determine the most estimable parameters from the measurements available and potentially design appropriate experiments to estimate the least estimable parameters.

The estimability analysis is based on the following matrix of sensitivities:

$$Z = \begin{bmatrix} s_{11}\big|_{T_1} & \cdots & s_{1n_p}\big|_{T_1} \\ \vdots & \ddots & \vdots \\ s_{n_s1}\big|_{T_1} & \cdots & s_{n_sn_p}\big|_{T_1} \\ s_{11}\big|_{T_2} & \cdots & s_{1n_p}\big|_{T_2} \\ \vdots & \ddots & \vdots \\ s_{n_s1}\big|_{T_k} & \cdots & s_{n_sn_p}\big|_{T_k} \end{bmatrix} \tag{12}$$

In this matrix, each column corresponds to the effect of a parameter on the outputs at different temperatures, for example. Each row corresponds to the effect of all parameters on one output for a given temperature.

The sensitivities are multiplied by scaling factors to ensure dimensional consistency and guarantee the same order of magnitude of the elements expressed as:

$$s_{ij}\big|_{T_k} = \frac{\bar{p}_j}{\bar{y}_i\big|_{T_k}} \frac{\partial \hat{y}_i}{\partial p_j}\bigg|_{T_k} \tag{13}$$

where $\hat{y}_i$ is the value predicted by the model which is determined by the vector of unknown parameters p, n_p is the number of unknown parameters, $\bar{p}_j$ is the nominal value of the j^{th} parameter taken from the literature or previous studies, and $\bar{y}_i\big|_{Tk}$ is the estimation of the i^{th} output, obtained using the nominal vector of the parameters $\bar{p}$.

The Z matrix is implemented within the estimability algorithm developed by Yao et al., (2003) in order to rank the parameters. It consists of the following steps:

(i) Calculate the module of each column of the Z matrix.
(ii) Choose the first estimable parameter corresponding to the column with the highest module.
(iii) Create an X_L matrix (vector in the first iteration), containing the Z column of the estimable parameter.
(iv) Calculate the Z_L matrix, which is the prediction of the Z sensitivity matrix, by using the subset of X_L columns, as follows:

$$Z_L = X_L \left(X_L^T X_L \right)^{-1} X_L^T Z$$

(v) Calculate the residual matrix R_L:

$$R_L = Z - Z_L$$

(vi) Calculate the module of each column of the R_L matrix. The column with the highest value corresponds to the next estimable parameter.
(vii) Increase the X_L matrix by adding the Z column of the new estimable parameter. The new matrix is called X_{L+1}.
(viii) Repeat steps (iv) to (vii) until the highest module value in the columns of the R_L matrix of residuals is smaller than a limit value (estimability threshold).

A parameter is considered to be non-estimable if the value of the module of its corresponding column in the Z matrix is less than a given estimability threshold. Its value is then taken from the literature or from previous studies.

The estimability threshold value is set in an almost arbitrary manner. Therefore, the number of estimable parameters depends significantly on the chosen value. In this work, the threshold value is set equal to 0.04 as in Yao et al. (2003), roughly meaning that for a parameter to be estimable, a variation of 10% of its value should cause at least a variation of 2 % of the model outputs. On the other hand, the elements s_{ij} of the Z matrix are local sensitivities, i.e., they depend on the initial values used for the unknown parameters, the resulting order of estimability of parameters may therefore change from one set of initial values to another. A more advanced method has recently been developed by Bouchkira et al. (2021) based on the works of Eghtesadi et al. (2013) and Saltelli et al. (2006).

The optimal values p^* of the most estimable parameters p^{est} are then determined by solving the following constrained optimization problem:

$$p^* := \arg\min_{P^{est}} \sum_{i=1}^{n} \sum_{j=1}^{k} \left(y_i^{mes} \Big|_{T_j} - y_i^{mod} \Big|_{T_j} \right)^2 \tag{14}$$

subjected to:

$$p_{\min}^{est} \le p^{est} \le p_{\max}^{est} \tag{15}$$

where y_i^{mes} and y_i^{mod} are the measured and predicted outputs, respectively.

The optimization algorithm used is based on the method of moving asymptotes (MMA) (Svanberg, 1987) available in Comsol Multiphysics ® software.

The accuracy of the identified parameters is assessed by means of confidence intervals (*CI*) given as:

$$p^*_{1-\alpha_t} = p^* \pm t_{s\left(n-n_p,\alpha_t/2\right)} \sqrt{diag(COV(p^*))} \tag{16}$$

where *COV* is the covariance matrix estimated using the following equation:

$$COV(p^*) \approx \frac{J^{mse}}{n-n_p} \left(J(p^*)^T J(p^*) \right)^{-1} \tag{17}$$

$t_{s_{(n-n_p,\alpha_t/2)}}$ is the Student *t*-distribution corresponding to the significance level $\alpha_t / 2$ and (n-n_p) degrees of freedom, J is the Jacobian matrix of the residue vector r_v, i.e. the difference between the predictions of the model and the measured values of the outputs expressed as:

$$J = \begin{bmatrix} \frac{\partial r_{v_1}}{\partial p_1} & \cdots & \frac{\partial r_{v_1}}{\partial p_{n_p}} \\ \vdots & \ddots & \vdots \\ \frac{\partial r_{v_n}}{\partial p_1} & \cdots & \frac{\partial r_{v_n}}{\partial p_{n_p}} \end{bmatrix} \tag{18}$$

Once the unknown parameters identified, the quality of the model predictions is assessed by means of the following performance indices:

-the root mean square errors (*RMSE*) between the model predictions and the experimental measurements, defined as (Shafeeyan et al., 2015):

$$RMSE = \sqrt{\frac{1}{nk}\sum_{i=1}^{n}\sum_{j=1}^{k}\left(y_{i|T_j}^{mes} - y_{i|T_j}^{mod}\right)^2} \tag{19}$$

- and the Pearson correlation coefficient (Benesty et al., 2009) expressed as:

$$r = \frac{\sum_{i=1}^{n}\sum_{j=1}^{k}\left(y_{i|T_j}^{mes} - \bar{y}_{i|T_j}^{mes}\right)\left(y_{i|T_j}^{mod} - \bar{y}_{i|T_j}^{mod}\right)}{\sqrt{\left(\sum_{i=1}^{n}\sum_{j=1}^{k}\left(y_{i|T_j}^{mes} - \bar{y}_{i|T_j}^{mes}\right)^2\right)\left(\sum_{i=1}^{n}\sum_{j=1}^{k}\left(y_{i|T_j}^{mod} - \bar{y}_{i|T_j}^{mod}\right)^2\right)}} \tag{20}$$

where n is the number of measurements, k represents the operating conditions (temperature, flow rate, or concentration, for example), $\bar{y}^{mes}$ and $\bar{y}^{mod}$ are the mean values of the measured and predicted data, respectively. Other indices can also be used (Willmott, 1981; Willmott et al., 1985; Ayawei et al., 2017) but do not lead to relevant information in our case.

5. Results and discussion

5.1. Adsorption isotherms

The estimability analysis algorithm using the forward orthogonalization algorithm of Yao et al. (2003) was applied to the Sips isotherm and led to the results presented in *Table 4*.

Table 4: Parameter estimability analysis of the Sips model

Rank	1	2	3	4	5	6
Parameter	q_{m0}	s_0	Q/R_gT_0	b_{s0}	χ	α
Iteration 1	3.81	1.12	0.77	1.05	0.027	0.006
Iteration 2	0	0.65	0.57	0.35	0.021	0.006
Iteration 3	0	0	0.55	0.35	0.018	0.003
Iteration 4	0	0	0	0.31	0.009	0.003
Iteration 5	0	0	0	0	0.008	0.003
Iteration 6	0	0	0	0	0	0.003

The estimability order of the parameters is as follows: $q_{m0} > s_0 > Q/RT_0 > b_{s0} > \chi > \alpha$. It is worth noticing that the last two parameters, χ and α, are not estimable based on the available experimental measurements and the estimability threshold value of 0.04. Therefore, their values were taken from one of our previous studies and set equal to 1.58 and 0.17 respectively (Cardenas et al., 2020; Bedel et al., 2017).

The four estimable parameters were then identified using the available experimental measurements. The optimal values, the confidence intervals at 95 %, and the correlation matrix are summarized in *Table 5* (the value of 285 K is used as the reference temperature). The tight confidence intervals show that the parameters are accurate and consistent with the values reported in the literature (Do, 1998; Bedel et al., 2017). On the other hand, the correlation matrix shows that the parameters are not strongly correlated. The same results are obtained in GAMS optimization environment using Baron global optimizer (Sahinidis, 1996).

Table 5: Identified parameter values of the Sips model

			Correlation matrix			
Parameters	Value	*CI* (95%)	q_{m0}	b_{s0}	s_0	Q/R_gT_0
$q_{m0,}$ (mol.kg^{-1})	2.98	±0.14	1			
$b_{s0,}$ (m^3.mol^{-1})	187.2	±41.8	-0.82	1		
s_0	1.96	±0.20	-0.59	0.14	1	
Q/R_gT_0	15.18	±1.61	0.34	-0.60	-0.07	1

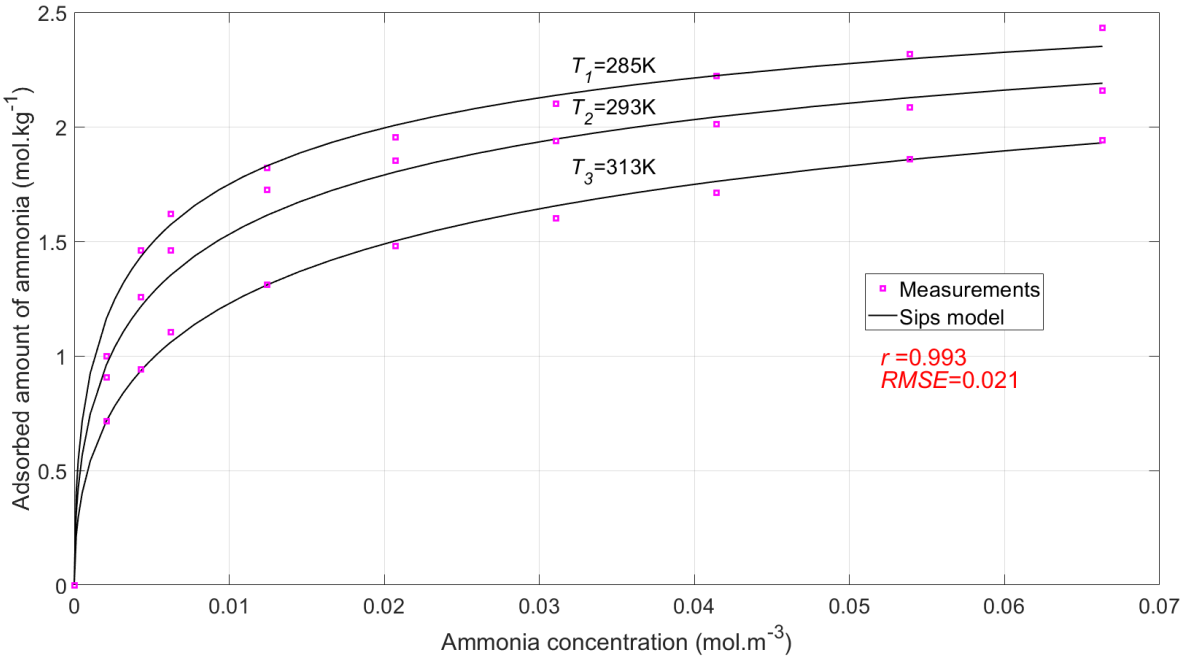

Figure 2: Comparison between Sips isotherm predictions and experimental measurements

Figure 2 shows the equilibrium adsorption isotherms of ammonia on zinc sulphate-doped activated carbon at 285, 293 and 313 K, with an ammonia concentration between 0 and 0.066 mol.m^{-3}. The high value of the Pearson correlation coefficient and the low value of *RMSE* demonstrate that the Sips isotherm is in very good agreement with the experimental measurements in the considered temperature and high ammonia concentration ranges. The resulting isosteric heat of adsorption at 285 K is equal to 36 kJ.mol^{-1} thus proving that ammonia

is likely to be chemically adsorbed. The isotherm so identified will be used later in the modeling of the adsorption process.

5.2. Breakthrough fronts

As with adsorption isotherms, the estimability algorithm of Yao et al. (2003) was applied to the model of breakthrough fronts involving three unknown parameters, i.e. k_{LDF}, c_{m_1} and c_{m_2}. The results obtained are presented in the following table:

Table 6: Parameter estimability analysis of adsorption models

Rank	1	2	3
Parameters	k_{LDF}, s^{-1}	c_{m_1}	c_{m_2}
Initial values	8×10^{-4}	0.18	0.008
Iteration 1	177	81.7	92.8
Iteration 2	0	71.9	64.1
Iteration 3	0	0	25.8

The analysis of these results shows that all parameters can be estimated from the available experimental measurements. The order of estimability is given as follows: $k_{LDF} > c_{m_1} > c_{m_2}$.

The experimental data used consist of breakthrough front measurements carried out at four different concentrations of ammonia (0.066; 0.054; 0.041 and 0.029 $mol.m^{-3}$) and three different gas flow rates (13.8, 9.0 and 4.4 $L.min^{-1}$), i.e. a total of 12 experiments to identify the parameters. The optimized values are presented in *Table 7*, as well as the confidence intervals (*CI*) at 95 % and the correlation matrix.

Table 7: Optimized parameter values of the ammonia adsorption model

			Correlation matrix		
Parameters	Value	*CI* (95%)	k_{LDF}, s^{-1}	c_{m_1}	c_{m_2}
k_{LDF} (s^{-1})	6.7×10^{-4}	$\pm2\times10^{-5}$	1		
c_{m1}	0.011	$\pm3\times10^{-3}$	-0.25	1	
c_{m2}	1.7×10^{-3}	$\pm6\times10^{-4}$	-0.31	-0.81	1

Here again, the tight confidence intervals show that the parameters were accurately determined with low correlation coefficients. The resulting axial dispersion coefficients (see *Table 8*) obtained for different gas flow rates are consistent with the literature data (e.g., Knox et al, 2016).

Table 8: Values of axial dispersion at different flow rates

Q_v, $L.min^{-1}$	D_{ax}, $m^2.s^{-1}$
13.8	0.016
9	0.011
4.4	0.007

Figure 3 compares the model predictions with the experimental measurements of breakthrough fronts at different concentrations of ammonia and gas flow rates, while all other parameters remain constant.

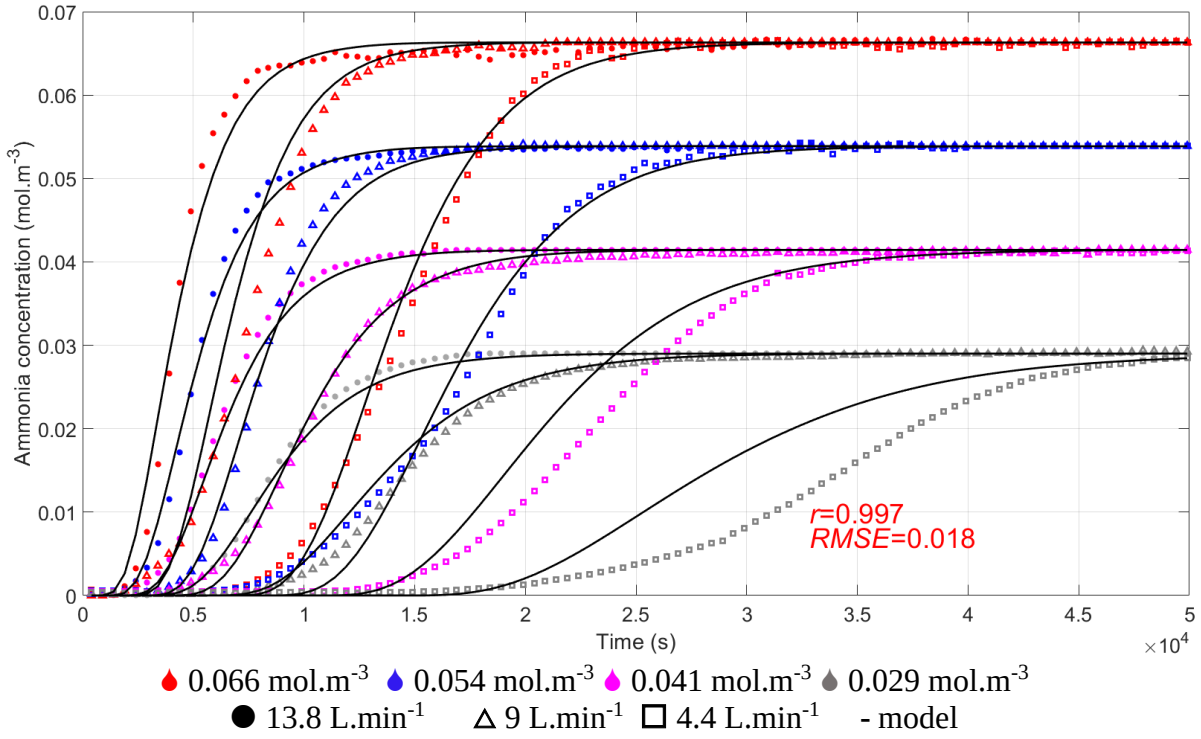

Figure 3: Comparison of breakthrough fronts predicted with the experimental data

It can be seen that the higher the increase of ammonia concentration and gas flow rate, the steeper the breakthrough front. On the other hand, the model predictions exhibit a good agreement with the experimental measurements. The relative disagreement at low flow rates and concentrations may be explained by the fact that it was very complicated to correctly supply the column with low concentrations, which increases the measurement errors. Despite these difficulties, the Pearson correlation coefficient (r = 0.997) was close to 1 and the root mean squares error (*RMSE* = 0.018) was very low, thus showing the good performance of the model.

The identified model was then validated using additional measurements of breakthrough fronts carried out at four gas flow rates of 25, 17, 13 and 7 L.min^{-1}, which were different from those used in parameter identification at an ammonia concentration of 0.041 mol.m^{-3}. The optimized values of the parameters presented in *Table 7* were used to compute the model predictions in the same operating conditions. *Figure 4* shows the comparison between the resulting predictions and the experimental data at different gas flow rates.

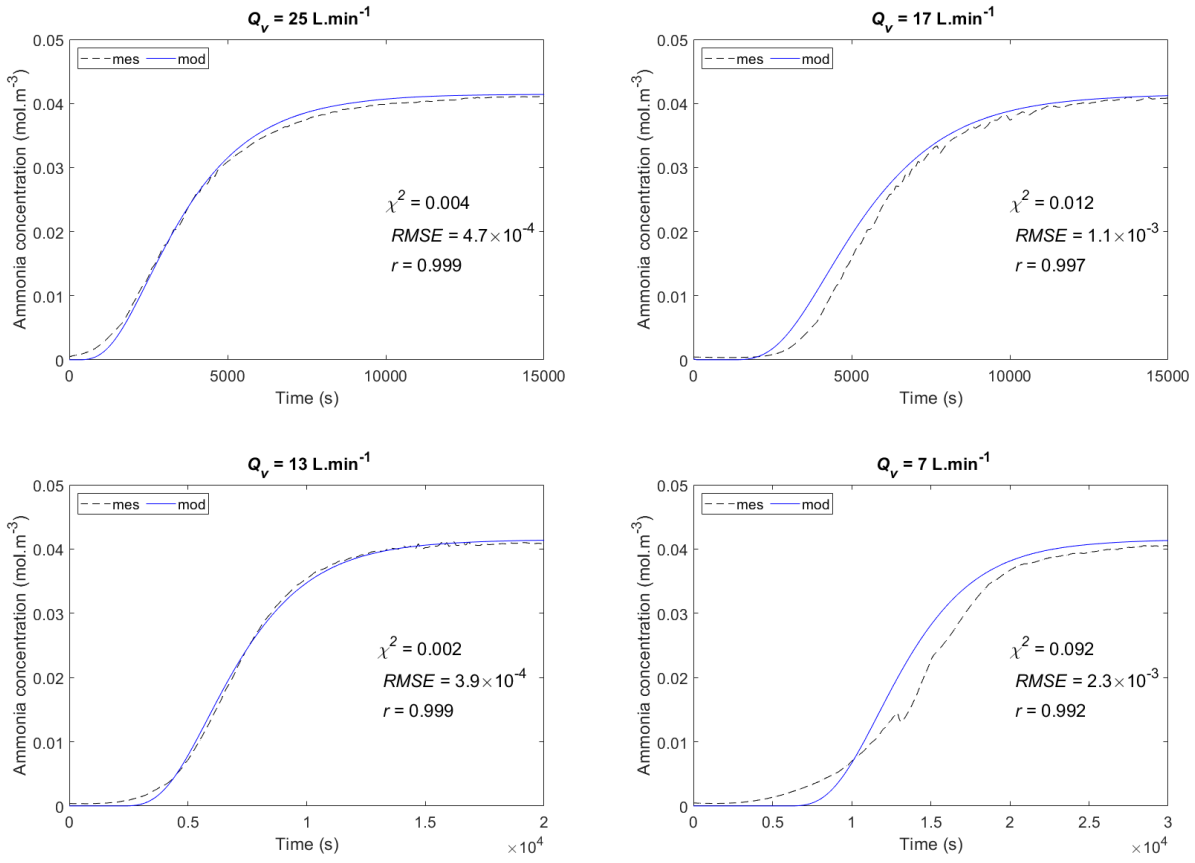

Figure 4: Comparison of predicted breakthrough fronts with experimental measurements at different flow rates.

The values of the Pearson correlation coefficient close to one and the very low values of *RMSE* index demonstrate that the gap between the experimental data and the model predictions is minimal. Furthermore, the chi-squared test was used to statistically validate the model. The null hypothesis (H_0) was defined as: the predicted and measured breakthrough fronts have the same distribution with the probability of 95%. The alternative hypothesis (H_1) is therefore: the predicted and measured breakthrough fronts do not have the same distribution with the probability of 95%. The observed chi-squared statistic is calculated by means of the following equation (Ayawei et al., 2017):

$$\chi^2 = \sum_{i=1}^{n} \frac{\left(y_i^{mes} - y_i^{mod}\right)^2}{y_i^{mes}} \tag{21}$$

where y^{mes} and y^{mod} are the measured and predicted values, respectively. The computed values of chi-squared are also reported in *Figure 4*.

On the other hand, the critical chi-squared value corresponding to the degree of freedom which is equal to the number of experimental measurements minus one, and to the significance level of the test (5%) was 3.84. It can be seen that all the computed values of the chi-squared are less than the critical value meaning that we cannot reject the null hypothesis (H_0), i.e., we can affirm with a probability of 95% that the predicted and measured breakthrough fronts have the same distribution.

The model that has been identified and validated can now be used as a tool to predict the saturation time of an ammonia adsorption column with doped activated carbon and to study the effect of different operating conditions such as temperature, concentration, flow rate, porosity, bed geometry, porosity, etc.

6. Conclusions

The accuracy and efficiency of the one-dimensional adsorption model developed, identified, and validated to simulate a fixed-bed column where ammonia is adsorbed on doped activated carbon was demonstrated. Therefore, it can be used in the design and optimization of industrial air purification boxes for mechanical devices.

However, the performance of the model can be further increased by improving in particular the equilibrium and transfer kinetics models. Indeed, the use of Toth's isothermal equation would better represent the equilibrium data, especially at low concentrations. Furthermore, since ammonia is likely to be adsorbed chemically, it would be interesting to investigate adsorption with chemical reaction using a Freundlich type isotherm. Moreover, the use of the advanced estimability analysis based on global sensitivities (Bouchkira et al, 2021), will allow us to compute the estimability threshold value for each parameter and determine the most estimable whatever their initial values.

Finally, the combination of these equilibrium equations with a multiscale model of mass transport in porous particles, would significantly improve the adsorption model and enable a better understanding of the mechanism of ammonia adsorption on doped activated carbon.

Nomenclature

c	Ammonia concentration (mol.m^{-3})
c_{m_1}, c_{m_2}	Constants to estimate the axial dispersion
c_{in}	Initial concentration of ammonia (mol.m^{-3})
D_{μ}	Intra-crystalline diffusion coefficient (m².s^{-1})
D_{AB}	Binary or molecular diffusion (m².s^{-1})
D_{ax}	Axial dispersion coefficient (m².s^{-1})
D_e	Effective porous diffusion (m².s^{-1})
D_K	Knudsen diffusion (m².s^{-1})
D_M	Mean diffusion of the mixture (m².s^{-1})
d_{pe}	Diameter of the activated carbon particle (m)
J^{mse}	Objective function
k_b	The Boltzmann constant (J.K^{-1})
k_H	Henry's law constant (-)
k_{LDF}	Overall LDF mass transfer coefficient (s^{-1})
M_A	Molecular weight of ammonia (kg.mol^{-1})
M_B	Molecular weight of air (kg.mol^{-1})
L	Bed height (m)
p_t	Total pressure (Pa)
Pe'	Péclet number
q_e^*	Quantity of ammonia adsorbed at equilibrium (mol.m^{-3})

Q_v	Flow rate ($L.min^{-1}$)
r_μ	Crystal radius (m)
Re_p	Reynolds number
r_{mp}	Macropore radius (m)
r_{pe}	Activated carbon particle radius (m)
T	Operating temperature (K)
T_0	Reference temperature (K)
v	Interstitial velocity ($m.s^{-1}$)

Greek letters

α_t	Level of significance
ΔH	Isosteric heat of sorption ($J.mol^{-1}$)
$\varepsilon_A, \varepsilon_B, \varepsilon_k$	Minimum value of the potential energy (J)
ε_b	Bed porosity ($m_g^3.m_{col}^{-3}$)
ε_{pe}	Particle porosity ($m_g^3.m_{pe}^{-3}$)
μ_B	Dynamic viscosity of air ($kg.m^{-1}.s^{-1}$)
ρ_g	Air density ($kg.m^{-3}$)
ρ_s	Solid density ($kg.m^{-3}$)
σ_A, σ_B	Characteristic length of the Lennard-Jones potential (m)
τ_{pe}	Tortuosity in the particle
Ω_D	Collision integral

References

Ayawei, N., Ebelegi, A. N., & Wankasi, D. (2017). Modelling and Interpretation of Adsorption Isotherms. *Journal of Chemistry*, *2017*, 11. https://doi.org/10.1155/2017/3039817

Bedel, S., Vallières, C., & Latifi, M. A. (2017). Parameters estimability analysis and identification for adsorption equilibrium models of carbon dioxide. *Adsorption*, *23*(2–3), 373–380. https://doi.org/10.1007/s10450-017-9864-7

Bémer, D., Courtois, B., Ferrari, P., & Silvente, É. (2015). Assainissement de l'air des cabines d'engins mobiles. In *Institut National de Recherche et de Sécurité* (Vol. ED6228).

Bémer, D., Lecler, M. T., Subra, I., Larrat, J. P., & Schaeffner, D. (2005). Performance of agricultural vehicle cabs pressurised against pesticides—aerosol testing method. *Biosystems Engineering*, *91*(3), 313–320. https://doi.org/doi:10.1016/j.biosystemseng.2005.04.007

Benesty, J., Chen, J., Huang, Y., & Cohen, I. (2009). Pearson correlation coefficient. In *Noise reduction in speech processing* (pp. 1–4). Springer, Berlin, Heidelberg. https://doi.org/https://link.springer.com/chapter/10.1007/978-3-642-00296-0_5

Bouchkira, I., Latifi, A. M., Khamar, L., & Benjelloun, S. (2021). Global sensitivity based estimability analysis for the parameter identification of Pitzer's thermodynamic model. *Reliability Engineering & System Safety*, *207*(107263), 1–14. https://doi.org/10.1016/j.ress.2020.107263

Brokaw, R. S. (1969). Predicting transport properties of dilute gases. *Industrial and Engineering Chemistry Process Design and Development*, *8*(2), 240–253.

https://doi.org/10.1021/i260030a015

Cardenas, C., Marsteau, S., Sigot, L., Vallières, C., & Latifi, A. M. (2020). Analysis of an Industrial Adsorption Process based on Ammonia Chemisorption: Modeling and Simulation. In *Computer Aided Chemical Engineering* (Vol. 48, pp. 625–630). Elsevier B.V. https://doi.org/10.1016/B978-0-12-823377-1.50105-1

Courtois, B., & Cadou, S. (2016). Valeurs limites d'exposition professionnelle aux agents chimiques en France. In *Institut National de Recherche et de Sécurité* (Vol. ED984).

Do, D. D. (1998). Adsorption Analysis: Equilibria and Kinetics. In *Chemical Engineering* (Vol. 2, Issue Imperial College Press). Imperial college press London. http://ebooks.worldscinet.com/ISBN/9781860943829/9781860943829.html

Eghtesadi, Z., Wu, S., & McAuley, K. B. (2013). Development of a model selection criterion for accurate model predictions at desired operating conditions. *Industrial and Engineering Chemistry Research*, *52*(35), 12297–12308. https://doi.org/10.1021/ie302408b

Glueckauf, E., & Coates, J. I. (1954). Formula for diffusion into spheres and their application to chromatography. *Journal of the Chemical Society (Resumed)*, *51*(10), 1315–1321. https://doi.org/10.1039/JR9470001315

Guimon, M. (2019). Les appareils de protection respiratoire. *Institut National de Recherche et de Sécurité*, *ED6106*, 64.

Králik, M. (2014). Adsorption, chemisorption, and catalysis. *Chemical Papers*, *68*(12), 1625–1638. https://doi.org/10.2478/s11696-014-0624-9

Millington, R. J., & Quirk, J. P. (1959). Permeability of porous media. *Nature*, *183*(4658), 387–388. https://doi.org/10.1038/183387a0

Neufeld, P. D., Janzen, A. R., & Aziz, R. A. (1972). Empirical equations to calculate 16 of the transport collision integrals Ω(l,8)* for the lennard-jones (12-6) potential. *The Journal of Chemical Physics*, *57*(3), 1100–1102. https://doi.org/10.1063/1.1678363

Organiscak, J. A., & Schmitz, M. (2012). *A new leak test method for enclosed cab filtration systems*. Department of Health and Human Services, Public Health Service.

Rastegar, S. O., & Gu, T. (2017). Empirical correlations for axial dispersion coefficient and Peclet number in fixed-bed columns. *Journal of Chromatography A*, *1490*, 133–137. https://doi.org/10.1016/j.chroma.2017.02.026

Rouquerol, J., Rouquerol, F., Llewellyn, P., Maurin, G., & Sing, K. S. W. (2013). Adsorption by Powders and Porous Solids. In *Principles, Methodology and Applications* (Second). Academic press. https://doi.org/10.1016/C2010-0-66232-8

Ruthven, D. (1985). Principles of adsorption and adsorption processes. In *Chemical Engineering and Processing: Process Intensification* (Vol. 19, Issue 2). https://doi.org/10.1016/0255-2701(85)80013-1

Sahinidis, N. V. (1996). BARON: A general purpose global optimization software package. *Journal of Global Optimization*, *8*(2), 201–205. https://doi.org/10.1007/bf00138693

Saltelli, A., Ratto, M., Tarantola, S., Campolongo, F., Commission, E., & others. (2006). Sensitivity analysis practices: Strategies for model-based inference. *Reliability Engineering & System Safety*, *91*(10–11), 1109–1125.

Shafeeyan, M. S., Daud, W. M. A. W., Shamiri, A., & Aghamohammadi, N. (2015). Modeling of Carbon Dioxide Adsorption onto Ammonia-Modified Activated Carbon: Kinetic Analysis and Breakthrough Behavior. *Energy and Fuels*, *29*(10), 6565–6577. https://doi.org/10.1021/acs.energyfuels.5b00653

Svanberg, K. (1987). The method of moving asymptotes—a new method for structural optimization. *International Journal for Numerical Methods in Engineering*, *24*(2), 359–373. https://doi.org/10.1002/nme.1620240207

Willmott, C. J. (1981). On the validation of models. *Physical Geography*, *2*(2), 184–194. https://doi.org/10.1080/02723646.1981.10642213

Willmott, C. J., Ackleson, S. G., Davis, R. E., Feddema, J. J., Klink, K. M., Legates, D. R., O'Donnell, J., & Rowe, C. M. (1985). Statistics for the evaluation and comparison of models. *Journal of Geophysical Research*, *90*(C5), 8995. https://doi.org/10.1029/jc090ic05p08995

Yao, K. Z., Shaw, B. M., Kou, B., McAuley, K. B., & Bacon, D. W. (2003). Modeling ethylene/butene copolymerization with multi-site catalysts: Parameter estimability and experimental design. *Polymer Reaction Engineering*, *11*(3), 563–588. https://doi.org/10.1081/PRE-120024426